Quarterly Progress Report

N01-NS-1-2333

Restoration of Hand and Arm Function by Functional Neuromuscular Stimulation

Period covered: July 1, 2004 to September 30, 2004

Principal Investigator: Robert F. Kirsch, Ph.D.

Co-Investigators:

Patrick E. Crago, Ph.D.
P. Hunter Peckham, Ph.D.
Warren M. Grill, Ph.D.
J. Thomas Mortimer, Ph.D.
Kevin L. Kilgore, Ph.D.
Michael W. Keith, M.D.
David L. Wilson, Ph.D.
Dawn Taylor, Ph.D.
Joseph M. Mansour, Ph.D.
Jeffrey L. Duerk, Ph.D.
Wyatt S. Newman, Ph.D.
Harry Hoyen, M.D.
John Chae, M.D.
Jonathon S. Lewin, M.D.
Dustin Tyler, Ph.D.

Program Manager: William D. Memberg, M.S.

Case Western Reserve University
Wickenden 407
10900 Euclid Avenue
Cleveland, OH 44106-7207
216-368-3158 (voice)
216-368-4969 (FAX)
rfk3@po.cwru.edu

Contract abstract

The overall goal of this contract is to provide virtually all individuals with a cervical level spinal cord injury, regardless of injury level and extent, with the opportunity to gain additional useful function through the use of FNS and complementary surgical techniques. Specifically, we will expand our applications to include individuals with high tetraplegia (C1-C4), low tetraplegia (C7), and incomplete injuries. We will also extend and enhance the performance provided to the existing C5-C6 group by using improved electrode technology for some muscles and by combining several upper extremity functions into a single neuroprosthesis. The new technologies that we will develop and implement in this proposal are: the use of nerve cuffs for complete activation in high tetraplegia, the use of current steering in nerve cuffs, imaging-based assessment of maximum muscle forces, denervation, and volume activated by electrodes, multiple degree-of-freedom control, the use of dual implants, new neurotization surgeries for the reversal of denervation, new muscle transfer surgeries for high tetraplegia, and an improved forward dynamic model of the shoulder and elbow. During this contract period, all proposed neuroprostheses will come to fruition as clinically deployed and fully evaluated demonstrations.

Summary of activities during this reporting period

The following activities are described in this report:

- *Intra-operative testing of nerve cuff electrodes*
- *Evaluation of the dynamic shoulder and elbow model*
- *Wireless data acquisition module for use with a neuroprosthesis*
- *An implanted neuroprosthesis for electrical stimulation through nerve- and muscle-based electrodes and myoelectric recording*

Intra-operative Testing of Nerve Cuff Electrodes

Contract sections:
E.1.a.i.4.3 Nerve Cuff Electrode fabrication and implantation

Summary

This quarter, the experimental setup to characterize the recruitment properties of the spiral nerve cuff electrode was validated. Matlab™-based software has been developed that is capable of generating full recruitment curves, consisting of approximately 20 data points, in less than one minute. The previously used clinical system (Epoch2000, Axon Systems, Hauppauge NY) collected one data point in about 2 minutes. It was, therefore, impossible to collect full recruitment information intraoperatively without the new clinical system. The same setup will also be used to characterize the electrodes chronically in a spinal cord injured subject to determine the full capabilities and limitations of the spiral nerve cuff electrodes.

Overview of Experimental Setup

The experimental setup (Figure 1) consists of five major components: preamplifiers, amplifiers, a stimulator, and a computer with data acquisition and custom software.

A set of preamplifiers were initially manufactured at our own facilities. These preamplifiers suffered from DC drift problems during EMG recording and were not adequate for this project. The problem was solved with commercially available preamplifiers (Figure 2, #BL-AE-WG, B & L Engineering, Tustin, CA).

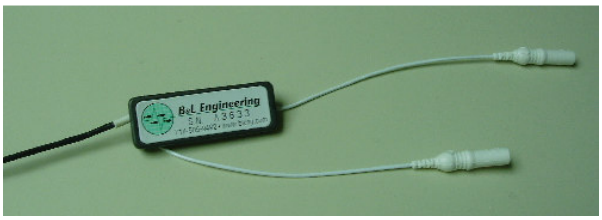

Figure 2. Pre-amplifiers from B & L Engineering.

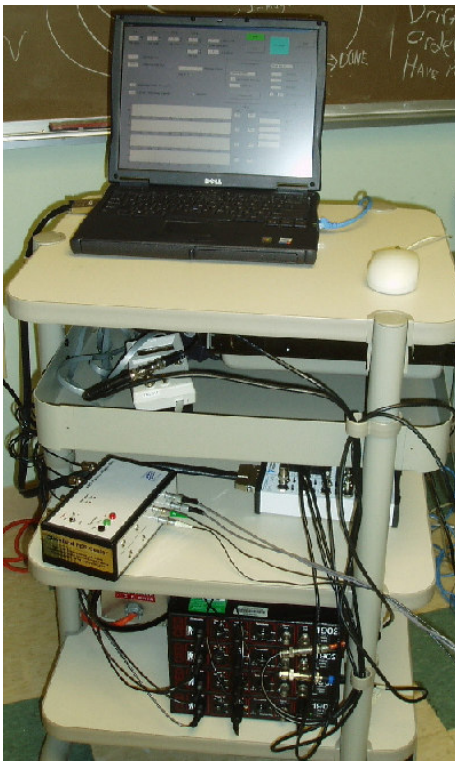

Figure 1. Intraoperative test setup

Four AC-coupled CED amplifiers (Model 1902, Cambridge Electronic Design, Cambridge England) amplified and low-pass (1 kHz) filtered the EMG signal. The CED amplifiers (Figure 3A) also clamped the input during stimulation to prevent saturation.

The stimulator is a custom specified four channel Crishtronics field-steering pulse generator (Figure 3B). This stimulator produces square, charge-balanced pulses with the capability of adding ramp pre-pulses and current steering. Finally, an eight-channel data acquisition board is installed in a laptop computer with the Matlab software installed.

Figure 3. A) Bank of four CED amplifiers.

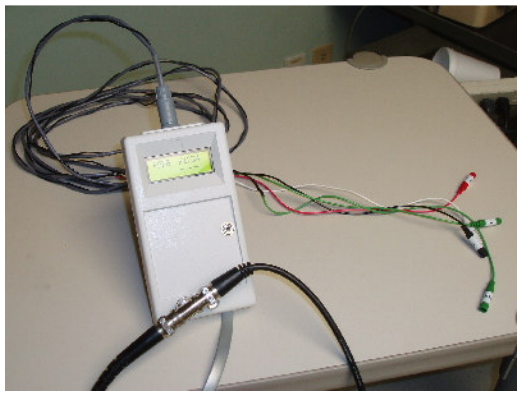

B) Crishtronics Stimulator.

The Matlab software (Figure 4) has three main functions. The first function allows the user to see the EMG response to one stimulus pulse. The stimulation parameters are specified and up to four channels of EMG response are displayed on the screen. The second function is a continuous running EMG response. A chain of pulses is sent at the specified stimulation frequency and each twitch response is displayed on the screen. The third function is the automatic generation of a recruitment curve. The inputs from the user are the stimulation channel, the modulation type, the range of values to modulate, and the required resolution of the curve. A binary search algorithm is used to locate discrete points along the curve with the specified resolution. Up to four recruitment curves can be generated simultaneously, and this

can be expanded to eight channels. This system makes it possible to collect large amounts of data intraoperatively and fully evaluate the selectivity of the spiral electrode.

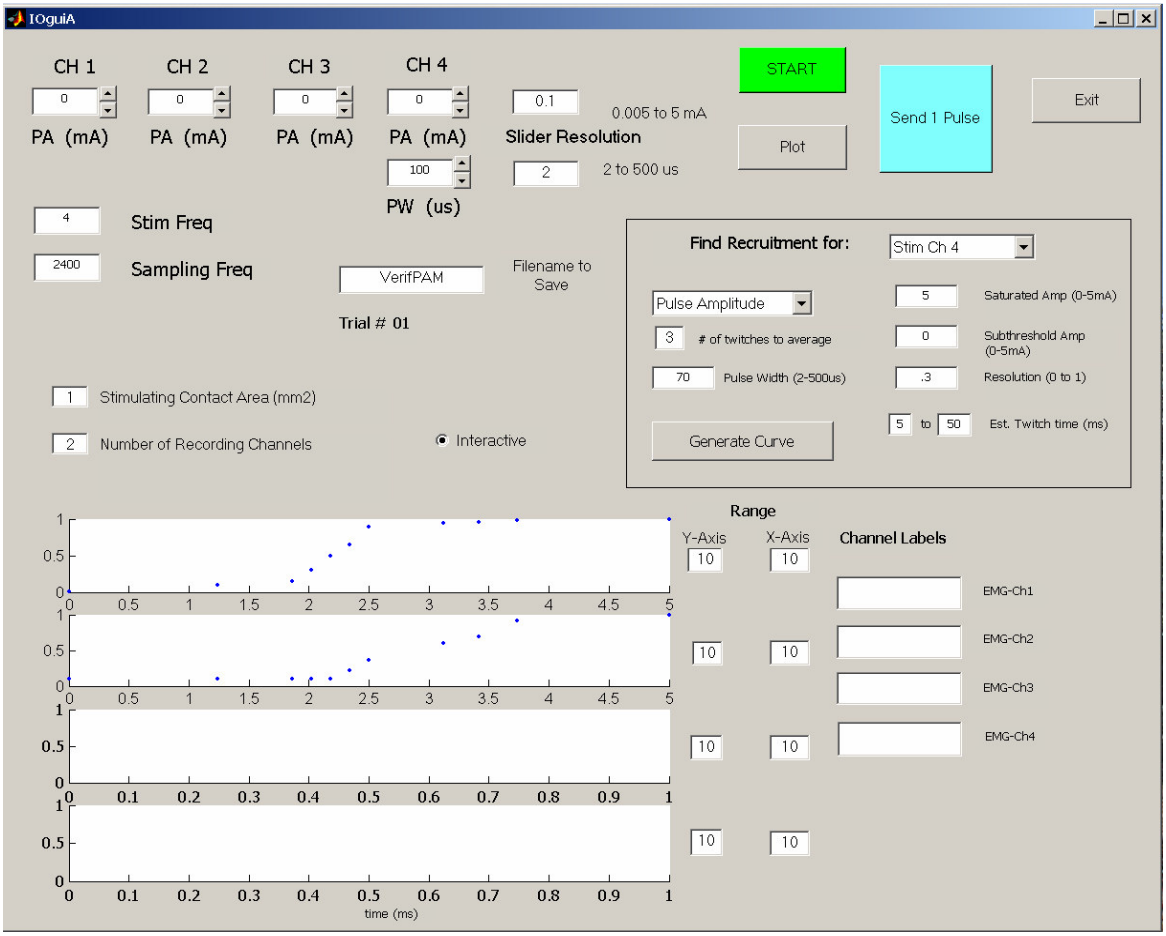

Figure 4. Matlab graphical user interface. Stimulation values are set in the upper left corner. Parameters for the recruitment curve generation are entered in the box at the right. Labels and axis ranges can be adjusted on the lower right and the responses are shown in the lower left.

Verification testing was performed to insure that the experimental system gave accurate results and could not cause harm to subjects. Two function generators were used to simulate muscle responses and the results were compared with the output of an oscilloscope.

Validation of Experimental setup and preliminary subject data:

Data was collected from one subject (subject 11) using the new experimental setup. Subject 11 had a central cord injury resulting in denervation of the proximal arm and shoulder muscles. A full recruitment curve was found for all four contacts of the spiral cuff electrode for both the median and ulnar nerve. Minimal muscle contraction was seen from the median nerve but sample recruitment curves from the ulnar nerve are shown below (Figures 5 & 6). The curves use pulse width modulation with the pulse amplitude set at 0.3 mA.

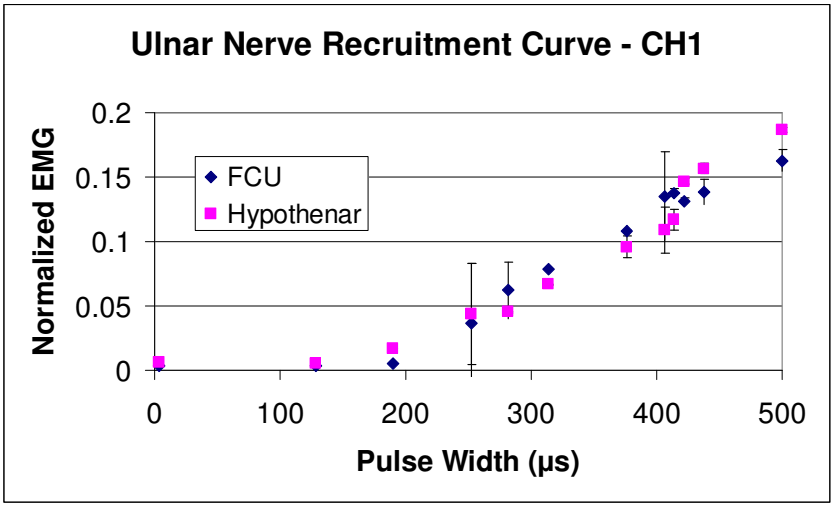

Figure 5. The FCU and hypothenar muscles are activated fairly equally and do not reach the maximal level with 0.3 mA, 500 us stimulation.

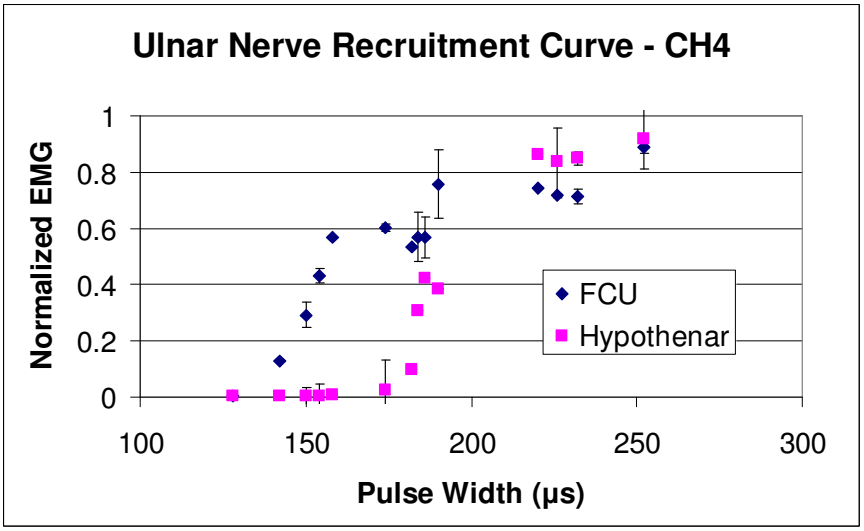

Figure 6. The FCU muscle is activated first and reached ~60% activation before the hypothenar muscle was recruited.

This data validates that the experimental setup generates accurate recruitment curves. In future subjects, a range of parameters will be tested and the resulting recruitment curves will be compared, allowing us to find the parameters that would activate each muscle individually. However, Figure 6 demonstrates the potential of this new software. It took approximately 2 minutes to generate recruitment curves for four positions around the nerve using the Matlab software while it took at up to 10 minutes to find the threshold value for each muscle at four positions using the Epoch2000 clinical system. This new experimental setup will be used during the next quarter to fully evaluate the selectivity of the spiral nerve cuff electrodes in additional subjects

Evaluation of the Dynamic Shoulder and Elbow Model

Contract section: E.1.a.ii.4.3 Development of forward dynamic model of human arm

Introduction

The development of a forward dynamic shoulder and elbow model was described in a previous Quarterly Progress Report (QPR#9, Apr-Jun 2003). As mentioned then, thorough validation of the model is not feasible because the muscle excitation patterns that are the model inputs are not directly measurable in the actual human arm. Thus, less direct indications of model accuracy must be examined. For his model of the upper extremity, van der Helm compared the predicted muscle forces with electromyographical (EMG) recordings (van der Helm 1994). Verification is thus achieved in an inverse dynamic manner, by comparing the timing of EMG activity in different muscles during arm movements with the activation patterns predicted by inverse dynamic simulations using the model. Qualitative agreement between the timing of measured and model-predicted muscle activations was obtained. The same method was chosen for the dynamic model described in this section.

Methods

Experiments to record arm movements in able-bodied subjects were conducted to obtain kinematic data and EMG recordings. The kinematic data was used as input to the shoulder and elbow model. After running inverse dynamic simulations, the model provided muscle activation patterns corresponding to the movements recorded. These activation patterns were compared to the EMG recordings to obtain a qualitative verification of the model.

Arm movements from able-bodied subjects were recorded using an Optotrak system (Northern Digital Inc.) that consists of three infrared cameras capable of recording the 3D positions of light emitting diodes (LEDs) located within the workspace. Sets of LED clusters were fixed over the thorax, upper arm and forearm of the subject. The locations of the scapula and clavicle were difficult to track dynamically, so a scapular palpator with a fourth cluster of LEDs was used to track the position of the scapula during static trials in different positions within the workspace [Veeger, et. al. 2003]. This data and the dynamic orientation of the humerus were used to recover the orientation of the scapula and the clavicle by regression that represents a standard shoulder rhythm [De Groot and Brand, 2001]. Specific bony landmarks were recovered during the movements in order to generate coordinate systems and obtain orientations for each joint in the shoulder and elbow. The recording and data processing were done following the International Shoulder Group recommendations for shoulder and elbow recordings [Van der Helm, 1997].

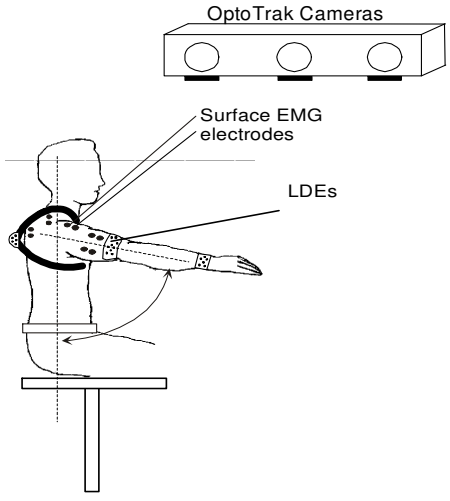

Figure 7. The experimental setup.

Electromyographic data was recorded from six muscles during the movements: biceps, triceps, anterior, middle and posterior deltoid, and upper

trapezius. These muscles were chosen because they are easily accessible through surface electrodes. The on-off patterns of the EMG were obtained after rectification and low pass filtering at a cutoff frequency of 4 Hz.

The movements performed included both single joint movements (shoulder abduction/adduction, shoulder flexion/extension, shoulder horizontal flexion/extension, shoulder internal/external rotation, elbow flexion/extension and forearm pronation/supination), and a set of functional movements comprised of activities of daily living (ADL) such as feeding, drinking, combing the hair, etc. Data was recorded at 50Hz. Figure 7 shows the experimental setup.

Results

Figure 8 shows an example of the analysis of a motion. The duration of this particular trial was 15 seconds and it consisted of four reaching movements above the shoulder level. The gray bands represent the time during which each muscle was active, according to the EMG recordings. The lines are the output of the inverse simulation, using the recorded kinematic data as input to the shoulder and elbow model. There is good agreement between the timing of the muscle activations predicted by the model and the timing of the EMG.

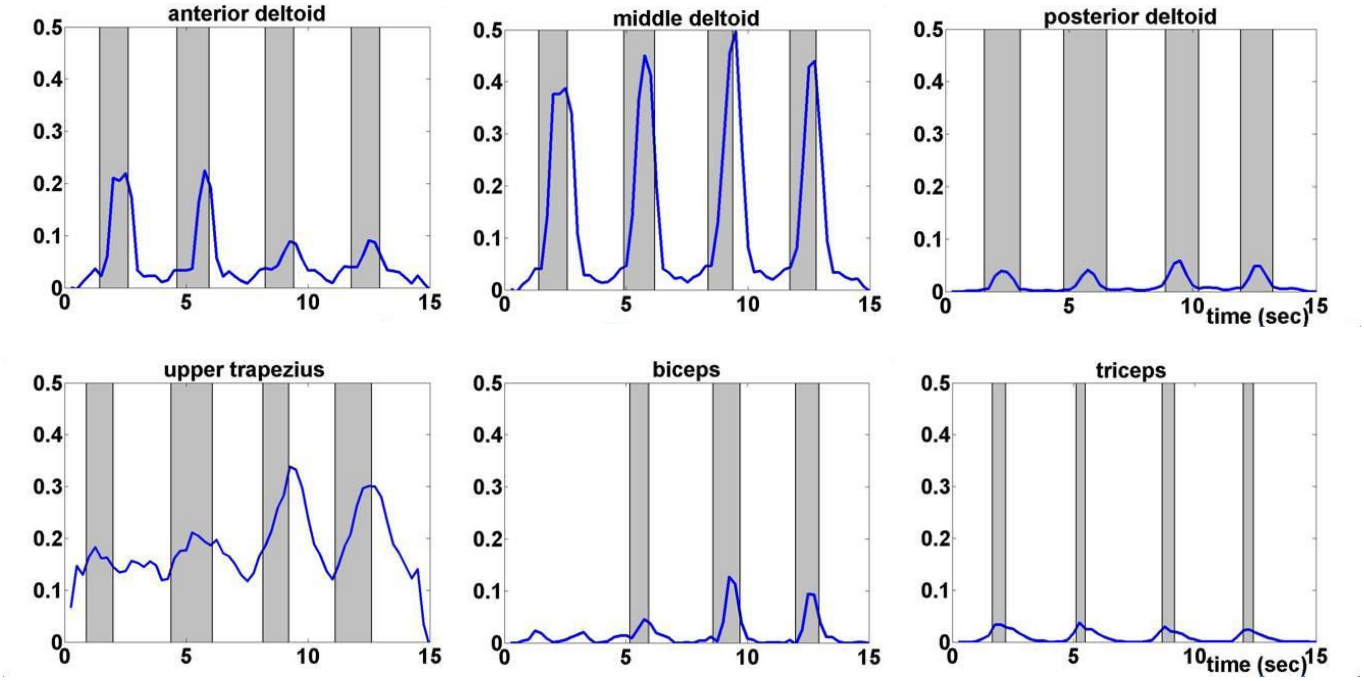

Figure 8. Comparison of model predicted activations (lines) with EMG on-off patterns (bands).

Next Quarter

In the next set of experiments, EMG data will be measured from more muscles. Percutaneous electrodes will also be used to reach deeper muscles and obtain better recordings.

References

De Groot, J.H., Brand, R. "A three-dimensional regression model of the shoulder rhythm" Clinical Biomechanics. Vol. 16 (2001), 735-743.

Van der Helm, F.C.T. "A finite element musculoskeletal model of the shoulder mechanism". Journal of Biomechanics. Vol 27. No 5. pp 551-569, 1994.

Van der Helm, F.C.T. "A standardized protocol for motion recordings of the shoulder". Proceedings of the First Conference of the International Shoulder Group, 1997.

Veeger,H.E.J., van der Helm, F.C.T., Chadwick, E.KJ., Magermans, D. "Toward standardized procedures for recording and describing 3-D shoulder movements". Behavior Research Methods Instruments & Computers. 35 (3). Pp 440-446, 2003.

Wireless Data Acquisition Module for Use with a Neuroprosthesis

Contract section: E.1.a.v Sensory feedback of contact and grasp force

Abstract

A general wireless data acquisition module (WDAM) is being developed for use with a neuroprosthesis. The WDAM is intended to be used with sensors such as the shoulder or wrist position transducer, finger-mounted joysticks, or remote on-off switches. Currently these sensors are connected to a controller via cables, which are cosmetically unappealing to the user and often get caught on wheelchairs, causing them to be damaged. Switch-activated transmitters mounted on walkers have been used previously in FES applications [1]. Recent advances in wireless technology have reduced the complexity and size of the wireless circuitry and have increased the likelihood that a small, low power, reliable wireless link could be assembled from commercially available components.

Methods

In the previous quarter, a printed circuit board (PCB) version of the WDAM was tested with different antenna types and different transmission rates, and a wireless joystick application was demonstrated. In the current quarter, more WDAMs were fabricated, and the WDAM's operating range, orientation sensitivity, and performance with different types of batteries were evaluated. In addition, quotations were obtained from two companies for the development of a miniature version of the WDAM.

WDAM fabrication

Ten additional PCBs were fabricated, with minor design changes from the previous version. Three of the PCBs were populated with components, including the "low-speed" version of the transceiver and the compact quarter-wave antenna (see previous Quarterly Progress Report, QPR#13, Apr-Jun 2004).

Transmission distance

Two of the newly assembled WDAMs were used in a 'master-slave' configuration. The master module requested data from the slave module, and used a CRC error-checking algorithm to determine if the proper data was received. The slave module was placed at distances of 1, 3, 5,

10, 20 and 30 feet from the master module (Figure 9). The measurements were made in a hospital laboratory, with no attempt to optimize the electromagnetic environment. For each test, 1000 data requests were sent, and the number and types of errors were counted and reported to a PC via a serial connection.

Transmission orientation

The setup for the orientation measurement was the same as for the distance measurements above, except that the slave module was placed at distances of 1, 3 and 5 feet from the master module at 30 degree increments around the module (Figure 9).

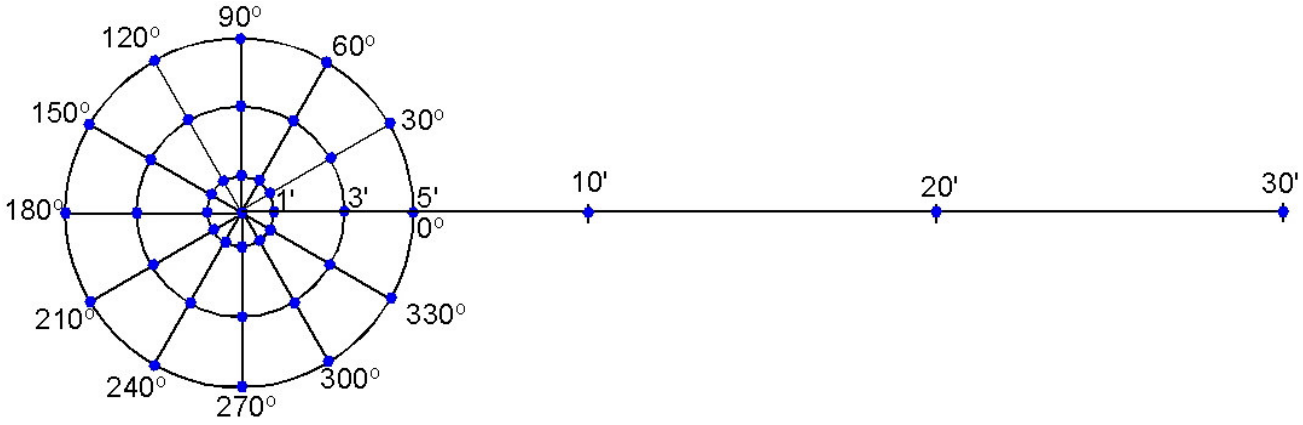

Figure 9. Distance and orientation measurement positions.

Battery longevity

Two different battery longevity tests were performed. The first one used the previously-selected zinc-air coin cell battery (Energizer 675, 1.4 V) and compared its longevity using the master-slave software protocol described above to the longevity using a "delta data" software protocol. In the "delta data" protocol, one WDAM transmits data only when an analog input changes by a pre-set threshold value. The transceiver is put into sleep mode when it is not transmitting. A second WDAM listens for the data and sends an acknowledgement when the data is received successfully. A 0.5 Hz square wave was used as the input signal to produce one data change per second.

The second set of longevity tests used the master-slave protocol and compared the zinc-air battery to two different lithium primary batteries (Duracell 1/3N, 3.2 V, and Tadiran BEL TL5186, 3.66 V). Since the zinc-air battery has a voltage of 1.4 V, the WDAM circuitry requires more current to produce the necessary 3.3 V supply, while less current is required from the 3.2-3.7 V lithium batteries. Although the capacity of the lithium batteries is less than that of the zinc-air battery, the lower current draw could make them last longer.

In both sets of tests, one of the WDAMs was serially connected to a PC, which recorded the status at 5 minute intervals.

Results

Transmission distance

The percentage of packets that were successfully acknowledged was consistently in the 90-97% range at distances of up to 20 feet (see Figure 10). At 30 feet, there was much more variability in the transmission success, ranging from 7% to 78%. This dropoff range is acceptable, since it is anticipated that the WDAM will be used at distances of less than 10 feet.

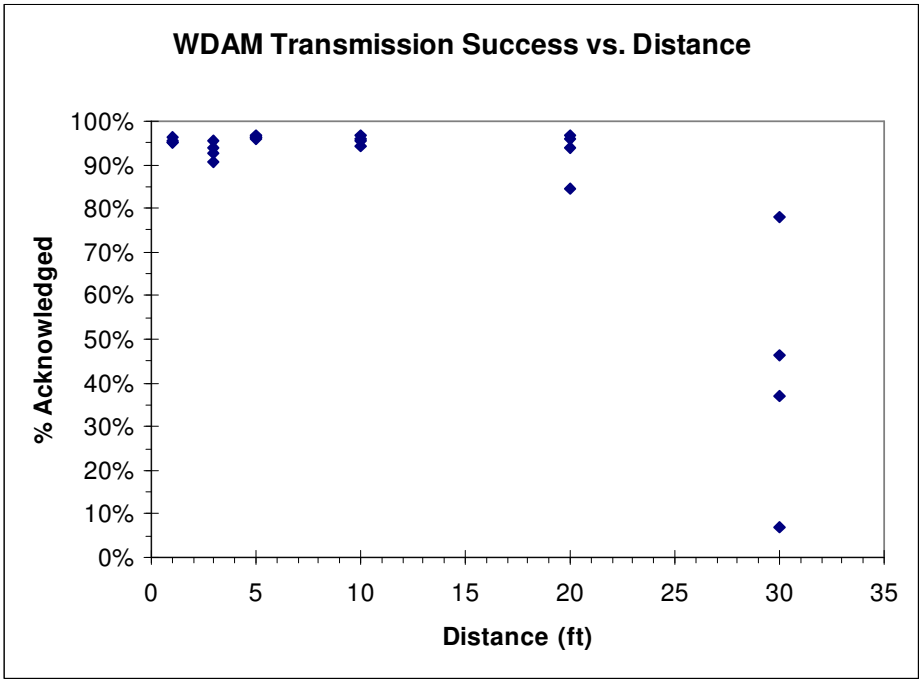

Figure 10. Packet transmission success vs. transceiver distance.

Transmission orientation

Except for the initial 3 measurements at the 0 degree position, the percentage of packets that were successfully acknowledged was consistently in the 93-97% range at all orientations (see Figure 11). The 3 measurements at the 0 degree position were repeated at the end of the experiment and were in the 93-97% range, so it is believed that there was a temporary RF noise problem that interfered with the measurements. These measurements will be repeated several times in the future to see whether this temporary decrease in the transmission success rate can be duplicated.

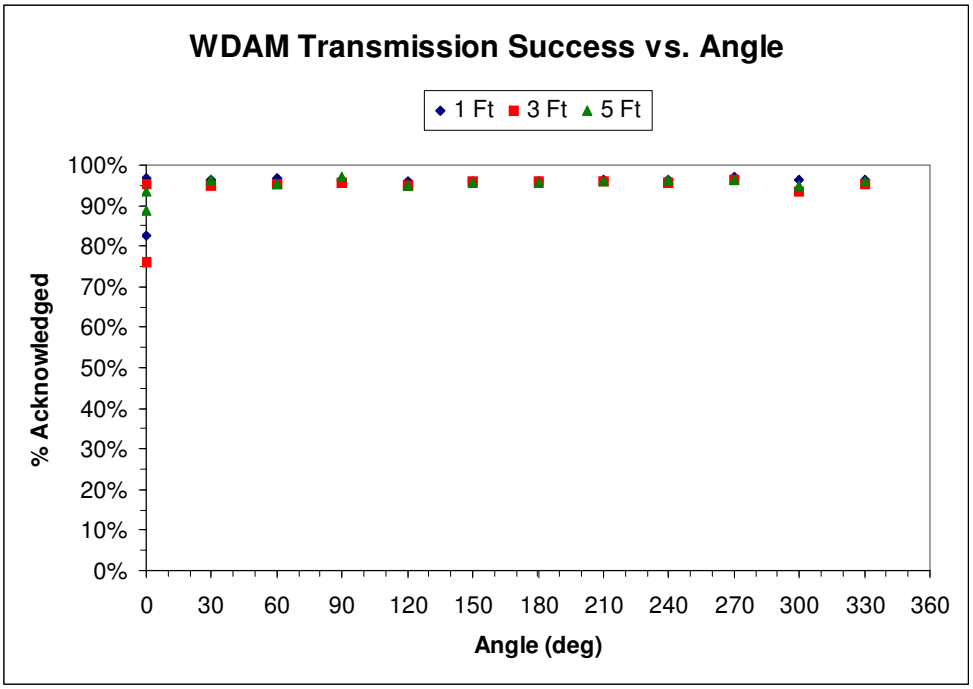

Figure 11. Packet transmission success vs. transceiver orientation.

Battery longevity

The results for the battery longevity tests can be seen in Table 1. The results from previously reported longevity tests are included for comparison. The "delta data" protocol resulted in the battery lasting 16% longer, presumably due to the transceiver being in sleep mode for short periods. This protocol should be an appropriate way to conserve power in applications where the data does not change very often (switches, for example).

Both lithium batteries provided much shorter operating times than the zinc-air battery. This is most likely due to the pulse amplitudes required by the WDAM. Even though the lithium batteries required much less current than the zinc-air battery, it still exceeded the nominal discharge currents recommended by the manufacturers.

Wireless Data Acquisition Module Battery Tests										
Battery Type	Brand	Model	Size (Diam. x Ht.) (mm)	Rated Capacity (mA-hr)	Starting Voltage (V)	Ending Voltage (V)	Protocol	Current Draw (mA)	Running Time (hrs)	Actual Capacity (mA-hrs)
Previous tests										
Zinc Air	Energizer	675	11.6 x 5.4	600	1.4	0.6	Master/slave	8.2	**74.1**	608
Lithium	Energizer	2032	20.0 x 3.2	225	3.2	0.9	Master/slave	3.0	**40.9**	123
Silver Oxide	Duracell	76S	11.6 x 5.3	175	1.6	0.1	Master/slave	6.3	**28.6**	180
Protocol Comparison										
Zinc Air	Energizer	675	11.6 x 5.4	600	1.38	0.99	Master/slave	9.5	**64.9**	617
Zinc Air	Energizer	675	11.6 x 5.4	600	1.37	0.95	Delta Data	8.7	**75.3**	655
Battery Comparison										
Zinc Air	Energizer	675	11.6 x 5.4	600	1.38	0.99	Master/slave	9.5	**64.9**	617
Lithium	Duracell	1/3N	10.8 x 11.6	160	3.25	0.93	Master/slave	3.4	**32.9**	112
Lithium	Tadiran	TL5186	22.5 x 7.5	400	3.66	0.97	Master/slave	3.2	**40.8**	131

Table 1. Battery longevity tests.

Miniaturization

Two manufacturers with experience in small electronics design and fabrication were provided with specifications for miniaturizing the WDAM. The design goal is to reduce the size to approximately a 1 inch square base, with the height depending on how many boards need to be stacked (1-3). Quotations were received from both companies and are currently being evaluated.

Next Quarter

In the next quarter, some of the transmissions tests will be repeated to see whether the decreased acknowledgement rate that occurred in a few of the orientation sensitivity measurements can be duplicated, and the cause identified. The ability to use multiple "slave" modules with one "master" module will be tested. We will investigate optimizing the data packet parameters and filter settings for the "medium-speed" and "high-speed" WDAM versions.

Also in the next quarter, we will select a manufacturer for the miniaturized WDAM, and work with them to produce several prototypes.

References

[1] Z. Matjacic, M. Munih, T. Bajd, A. Kralj, H. Benko, and P. Obreza, "Wireless control of functional electrical stimulation systems," *Artif Organs*, vol. 21, pp. 197-200, 1997.

An Implanted Neuroprosthesis For Electrical Stimulation through Nerve- and Muscle-based Electrodes and Myoelectric Recording

Contract section:

E.1.a.vi Implementation and evaluation of neuroprostheses for high tetraplegia

Introduction

The goal of this section of the project is to develop the hardware components necessary to implement advanced neuroprostheses for high tetraplegia. The key component of this effort is the development of an implanted stimulator/telemeter device that is capable of both electrical stimulation and myoelectric recording. Specifically, we are designing and fabricating an implanted neuroprosthesis that is capable of 12 channels of stimulation and has two channels of myoelectric signal (MES) recording, referred to as the implantable stimulator-telemeter-12 (IST-12). The myoelectric signal recording has been successfully demonstrated in-vivo, and is now being implemented with human subjects (in a separate project). With this phase of development completed, we are now addressing the specific stimulation capabilities of this device that are needed for this contract. Specifically, the device must be capable of safely and effectively delivering stimulus parameters that are appropriate for stimulation using muscle-based electrodes **and** nerve-based electrodes. During this quarter, we incorporated into the new circuit the design changes for both the cuff electrode current amplitudes and the recharge interrupt. We also had circuit boards fabricated for final stimulator assembly.

Design Modifications

The IST circuit has been modified to correctly and safely stimulate nerves. The IST generates current amplitude from four internal source channels. These sources can then be summed to create the desired output. In IST Rev A devices, the sources were set at 2.5 mA, 2.5 mA, 5 mA and 10 mA. These values have been updated to 0.1 mA, 0.7 mA, 1.3 mA, and 17.9 mA. The output current level is selected with three bits of information, which determine which sources to sum. Table 2 summarizes the eight available current levels in both Rev A and Rev B designs. As shown, the lowest current level available is now 0.1 mA, and the lowest four output levels are all suitable for safe nerve-based stimulation (less than 2.5 mA) while the upper four levels remain adequate for muscle-based stimulation. This change will be used in all IST family devices requiring nerve stimulation capability.

Bit Code	Sources	Rev A out	Rev B out
000	A only	2.5 mA	0.1 mA
001	A+B	5.0 mA	0.8 mA
010	A+C	7.5 mA	1.4 mA
011	A+B+C	10 mA	2.1 mA
100	A+D	12.5 mA	18 mA
101	A+B+D	15 mA	18.7 mA
110	A+C+D	17.5 mA	19.3 mA
111	A+B+C+D	20 mA	20 mA

Table 2. IST current amplitudes.

In addition, the IST high voltage power supply circuit was modified with the addition of a diode to interrupt the control signal when any stimulus channel was actively stimulating in the cathodic phase.

Results

Modifications to the IST circuit were made to address the nerve electrode current amplitude and anodic stimulation limitations of the previous design. The original layout and subsequent circuit board footprint could accommodate these modifications, so the design was sent to a subcontractor for fabrication. Ten such circuits were made for the IST-16 device, and 15 circuits were made for the IST-12 device. These circuits are currently testing satisfactorily, and the culmination of this effort will be 6 IST devices this quarter.

Conclusion

The IST circuit was modified to address two limitations of the previous design. These changes were finalized and circuit boards fabricated during this quarter. The circuits are undergoing final inspection, and up to 6 IST devices will be finished during the next quarter.